

## MODELLING SLOSHING IN LNG TANKS

Murray RUDMAN and Paul W. CLEARY

CSIRO Mathematical and Information Sciences, Private bag 33 Clayton South, Victoria 3169, AUSTRALIA  
Corresponding author, E-mail address: Murray.Rudman@csiro.au

### ABSTRACT

The Smoothed Particle Hydrodynamics (SPH) method is applied to the problem of modelling sloshing in a two-dimensional water model that is a representation of a scaled LNG tank. One configuration, which is a transverse slice through a membrane type tank, is studied here. Two fill levels (20, 70%) and two different oscillation amplitudes (10 and 20% of the tank dimension) are considered. Predicted pressure signals are compared to experimental measurements. The peak pressure values predicted in the simulations are generally lower than the experimental values, although they are the correct order of magnitude. The stochastic nature of the oscillations in practice means that an exact match between simulation and experiment is not feasible. Ensemble averaged pressure traces and standard deviations of the pressure from the simulation results are also presented. They show generally higher variability in the pressure signals for low fill ratio compared to high fill. The magnitude of fluctuations is also sensitive to the sensor location. SPH provides results for the peak pressures that are the correct order of magnitude on average, although the highest peaks are under-predicted. It is a natural technique for such coupled fluid-structure problems with large free surface deformations.

### INTRODUCTION

Sloshing in partially filled LNG tanks can arise under different ocean wave conditions. Examples include when loading and/or unloading LNG from a tanker ship, when tankers must disengage part way through offshore loading due to adverse weather conditions or in FPSO's under normal operating conditions. Sloshing may resonate with structural frequencies and those of wave-induced ship motions. This can subsequently affect ship stability and, of particular importance here, can produce large loads on the internal tank membranes. In turn this can lead to structural damage to tank membranes and insulation, leakage and potentially to tank rupture.

Small-scale physical experiments can be undertaken with water or other fluids and then scaled up to full size to predict tank loadings under different assumed wave conditions and fill levels. However it is highly desirable to have robust computational tools that provide accurate estimates of loadings under different conditions. Not only do computational methods allow a quick turn around for investigating different tank geometries, wave conditions and fill levels, it is also possible to apply the correct equations of state for liquid LNG when modelling. The use of LNG in experiments is problematic due to the difficulty in making measurement at very low

temperatures as well as the significant safety issues when using liquid LNG.

The non-linearity of fluid motions when the forcing amplitude becomes large combined with the possibility of free surface overturning, fragmentation and entrainment of a gaseous phase all indicate that simplified computational approaches (e.g. potential flow methods) are inadequate in the general sloshing case. Thus an appropriate numerical method must be able to handle arbitrary, complex free surface behaviour. There are two main classes of methods able to handle such complexity:

- Interface capturing techniques (examples are Volume-of-Fluid (VOF) originally developed by Hirt and Nichols (1981) and Level Set methods, Sussman *et al.* (1994)); and
- Smoothed Particle Hydrodynamics (SPH) originally developed by Gingold and Monaghan (1977) and then extended to free surface incompressible flows by Monaghan (1994).

An increasing number of numerical investigations of sloshing have appeared in recent years. A selection of these are the papers of Wemmenhove *et al.* (2007), Jung *et al.* (2008), Schreier and Paschen (2008), Singh *et al.* (2008) and von Bergheim and Thiagarajan (2008). The majority of these studies use either commercial software (CFD/Fluent/MSc.Dytran) coupled to a VOF technique or purpose built VOF codes such as the ComFlow code (Gerrits and Veldman, 2003).

In this paper we apply the Smoothed Particle Hydrodynamics technique to model the two-dimensional sloshing systems specified in Kim *et al.* (2009). These systems were thin-slice scaled water models that were instrumented to allow measurement of pressure signals in the tank and a number of different locations.

SPH is a computational technique that has been widely applied to industrial and environmental flows (e.g. Cleary 1998, Cleary and Prakash 2004). It has more recently been applied to oceanic and offshore hydrodynamics (see for example Gomez-Gesteira 2005, Shao 2006, Cleary and Rudman 2009).

### MODEL DESCRIPTION

Unlike most numerical techniques for Computational Fluid Dynamics, SPH does not utilize a fixed nodal grid. Instead, the grid is replaced by a set of moving points (or "particles") on which the discretised equations are solved. Each particle carries mass, momentum and energy and moves with the local fluid velocity. There is no explicit connectivity of the particles which means, for example, that particles that are close neighbours at one instant in

time can be quite distant from each other at a later time. Also, because the particles are transported with the local fluid velocity, the non-linear terms that usually appear in the momentum equations in grid-based methods are replaced by time derivatives following the particle motion. A detailed description of the method can be found in Monaghan (1994) and an outline of the implementation for sloshing is provided in Rudman *et al.* (2009). A minimal description of the method is included here for completeness.

### Interpolation

SPH interpolation allows a continuous function of the spatial variables to be defined as an interpolant of the discrete values at the particle positions. This is approximated by a summation over the nearby particles  $i$  as:

$$F(\mathbf{r}) = \sum_i m_i \frac{F_i}{\rho_i} W(\mathbf{r} - \mathbf{r}_i, h) \quad (1)$$

Here  $m_i$  is the mass of particle  $i$ ,  $F_i$  the associated discrete value of the field  $F$ , and  $\rho_i$  the particle density calculated from a transport equation described below. The smoothing length,  $h$ , is chosen such that the integration is performed over a volume that has a radius larger than the mean particle spacing by a factor of two or more. The discrete form of the spatial derivative of an interpolated quantity needed in the equations of motion is:

$$\nabla F(\mathbf{r}) = \sum_i m_i \frac{F_i}{\rho_i} \nabla W(\mathbf{r} - \mathbf{r}_i, h). \quad (2)$$

The choice of interpolation kernel  $W(r-r_i, h)$  is discussed in Monaghan (1992).

### Equations of Motion

The equation for mass transport is written in SPH form as

$$\frac{d\mathbf{r}_i}{dt} = \mathbf{v}_i + 0.5 \sum_j m_j \frac{\mathbf{v}_j - \mathbf{v}_i}{0.5(\rho_j + \rho_i)} W_{ij} \quad (3)$$

(where  $W_{ij} = W(r_j - r_i, h)$ ). The particle density  $\rho_i$  is calculated from the transport equation:

$$\frac{d\rho_i}{dt} = \sum_j m_j (\mathbf{v}_i - \mathbf{v}_j) \cdot \nabla W_{ij} \quad (4)$$

The equation for momentum transport is written

$$\frac{d\mathbf{v}_i}{dt} = - \sum_j m_j \left( \frac{P_i}{\rho_i^2} + \frac{P_j}{\rho_j^2} + \Pi_{ij} \right) \nabla_i W_{ij} \quad (5)$$

where  $\Pi_{ij}$  is the viscous term:

$$\Pi_{ij} = \frac{\xi}{\rho_i \rho_j} \frac{4\mu_i \mu_j}{(\mu_i + \mu_j)} \frac{\mathbf{v}_{ij} \cdot \mathbf{r}_{ij}}{\mathbf{r}_{ij} \cdot \mathbf{r}_{ij}}. \quad (6)$$

Here  $\mathbf{r}_{ij} = \mathbf{r}_i - \mathbf{r}_j$ ,  $\mathbf{v}_{ij} = \mathbf{v}_i - \mathbf{v}_j$  and  $\xi$  is a factor that varies with dimension and the details of the kernel (see Cleary, 1998 for details).

SPH utilizes an equation of state to define the pressure and here we use the stiff equation of state

$$P = P_0 \left( \frac{\rho}{\rho_0} - 1 \right)^\gamma. \quad (7)$$

with  $\gamma$  chosen here to be equal to 7. This choice results in density variations in the fluid that are typically less than 1% of the fluid density. The Courant number (defined

using the speed of sound and mean particle spacing) is 0.5. Based on typical fluid flow velocities this corresponds to a Courant number of 0.05. Time-stepping is by use of a second-order Improved Euler scheme. Convergence of the method with changes in particle spacing has not been addressed for this configuration, however previous work (Monaghan 1992) indicates that the method is 2<sup>nd</sup> order in space.

### Pressure predictions

The walls of the LNG tank are discretised using a special set of SPH boundary particles whose positions are fixed relative to each other. This ensemble of particles prescribes a path defined by the desired tank motion (roll, pitch, sway, etc). The boundary particles repel any fluid particles that approach them using a ‘‘Lennard-Jones’’ potential (see Cleary 1998). The pressure on the tank wall is determined by calculating the normal force applied to the boundary particles and dividing by the particle’s equivalent ‘‘surface area’’. Because the boundary force is only ever repulsive, when fluid particles move away from the zone of influence of the wall, they apply no force to the wall. Importantly, in cases where there could be ‘‘suction’’ on the wall and hence negative pressure, the SPH wall force will be calculated as zero, as will the wall pressure. Thus it is seen below that the SPH pressure sensor values never become negative, unlike the experimentally measured values. This aspect of the modelling requires improvement in future to allow negative pressures to be predicted when applicable.

### Computational details

Details of the tank geometry and sensor locations can be found in Kim *et al.* (2009) and will not be repeated here. Schematically, the tank configuration is shown in Figure 1 and is the octagonal or ‘‘transverse model’’ of Kim *et al.* It is an approximation of a 2-D slice through a scaled 3D membrane type LNG tank. The mean particle spacing in the simulations here was chosen to be  $h = 10$  mm and material parameters are those for water. In this preliminary study, the particle spacing was not varied to check on the convergence of the method with resolution, and this aspect of the simulations must be addressed in the future.

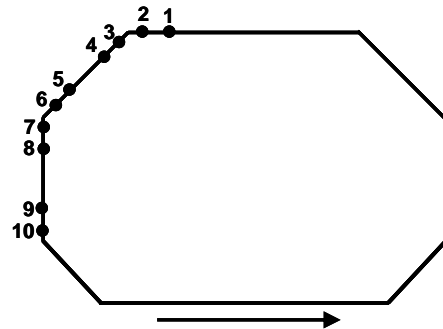


**Figure 1:** Schematic of tank geometry and sensor locations. The arrow indicates the direction of initial tank motion.

The tanks is oscillated in the  $x$ -direction (mimicking sway motion in a real LNG carrier) with the  $x$ -component of the tank velocity is given by

$$v = 2\pi f A \sin(2\pi f t). \quad (8)$$

Here,  $f$  and  $A$  are the oscillation frequency and motion amplitude (in metres). Details are given in Table 1 where it is noted that the two different amplitudes for tank correspond to 10 and 20% of the tank dimension in the direction of oscillation.

**Table 1** Parameters for simulations

$A$ (metres)	%Fill	$f$ (Hz)
0.151 and 0.303	20	0.4632
	70	0.6861

Time-averaging was used during pressure data collection with a time-scale equal to approximately three acoustic time-scales ( $\tau=h/c_s$ ) of the method. The equivalent simulation data acquisition frequency is approximately 1 kHz, which is lower than the experimental measurement frequency (20 kHz), hence we expect to miss the larger peaks that can be detected in the experiments. This signal still contained a level of noise and was further smoothed with one pass of an 11-point running average filter in time.

In addition to the time varying pressure signals, an ensemble-averaged (or phase-averaged) pressure signal was calculated from all data collected after the first five oscillation periods. This average illustrates the general behaviour of the pressure although in it will not reveal the maximum peak values that will be smoothed by averaging. From this ensemble average, a standard deviation of the pressure trace was also calculated. Like the ensemble average, this is a time-trace over one period, with the deviation at any time in the phase calculated with respect to the ensemble average at that time. The sloshing system considered here contains a significant stochastic component and we do not expect to get perfect agreement between experiment and simulation. However the ensemble-average pressure and standard deviation provide statistical information that could be used to compare simulation and experiment in a statistical way.

#### Experimental pressure traces

At the time of writing, the experimental data was unavailable for direct comparison. A select number of experimental pressure traces were manually digitized from the plots presented in Kim *et al.* (2009) in order to compare the with the simulation results. As a consequence, they are imprecise. However, they correctly show the phase of the experimentally measured signal and the maximum pressures measured as well as providing an approximately correct shape.

## RESULTS

### 20% fill level

Sequences of fluid distribution for the two different amplitude oscillations (151 and 303 mm) for one half of a typical period are shown in Figure 2 for the 20% fill level. Start-up pressure sensor readings for sensor #9 are compared to experimental traces in Figure 3. Ensemble-averaged pressure traces and the standard deviation of the ensemble for sensors #9 and 10 are shown in Figure 4. (Note that sensors #5, 6, 9 and 10 were the only sensors used in the experiments and hence simulations.)

The behaviour for the two different amplitudes with 20% fill are qualitatively similar (Figure 2). At maximum

horizontal displacement to the left (top row) the fluid on the bottom of the tank has impacted the left-hand wall and has just started forming a vertical jet (151 mm amplitude) or the jet is well formed and is approaching the filet on the tank wall (303 mm impact). Note that the acceleration toward the right is maximum at this time. The pressure of impact combined with a near maximum in wall acceleration leads to the peak pressure occurring at this phase of the oscillation. As the tank moves to the right, the acceleration reduces and this jet starts to collapse. The pressure at sensors #9 and #10 then begins to drop. At around the point of zero mean displacement (and maximum velocity), the collapsing column forms a small overturning wave before impacting on the right-hand wall (not shown) and the sequence is repeated.

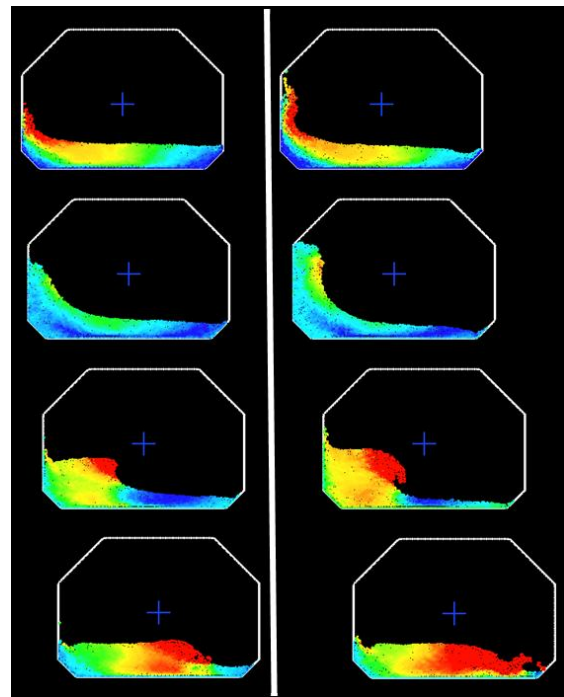


**Figure 2:** Fluid particle positions for 20% fill (151 mm amplitude left column and 303 mm right column). The first half of the oscillation period is shown as the tank moves from left to right. The maximum velocity (red) is associated with the wave tip and is equal to  $2.25 \text{ ms}^{-1}$  for 151 mm amplitude and  $3.0 \text{ ms}^{-1}$  for 303 mm amplitude.

For the low amplitude oscillation (151 mm), the fluid only occasionally reaches sensors #5 and 6 (on the lower side of the upper filet) and only just reaches them regularly for the high amplitude case (303 mm) inducing pressures of the order 1 kPa, hence details of these traces are not discussed.

Despite the strict periodicity of the tank oscillation, the predicted pressure peak varies significantly from period to period. This can be seen in the traces shown in Figure 3 and the ensemble-averaged signals in Figure 4. The pressure signal for this case is quite noisy, with pressure maxima at location #9 typically around the 3-5 kPa (4-8 kPa) for 151 mm (303 mm) amplitude. The peak pressures predicted by SPH are in reasonable agreement with those measured experimentally, although the stochastic nature of the sloshing results in predictions for individual peaks that have different magnitude to the

measurements. For the low amplitude oscillation, the predicted peaks are approximately 10-20% lower than the measurements. For the high amplitude the predicted are generally a little lower than measured except for the first 3-4 peaks. The phase of the pressure peak is generally in good agreement with the experiment although there are some discrepancies. The most noticeable difference between simulation and experiment is the absence of negative pressures in the simulation results. The reasons for this have been discussed above in the section on the computational method.

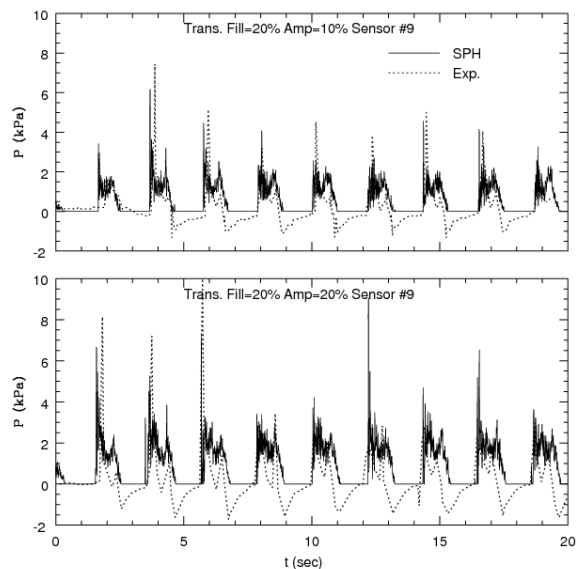


**Figure 3:** Pressure signal at start-up for at sensor locations #9 for 20% fill level in the transverse tank: 151 mm amplitude (top) and 303 mm amplitude (bottom). SPH results (solid line) are compared to experimental results (dashed line).

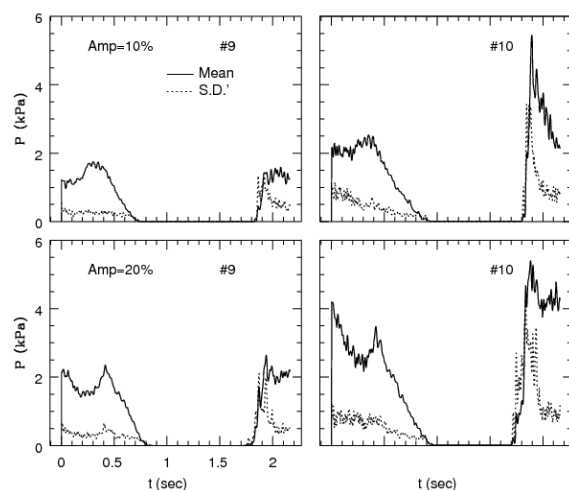


**Figure 4:** Ensemble averaged pressure trace and standard deviation for sensors #9 and 10 for the transverse tank with 20% fill: Solid line is the ensemble-averaged pressure trace and the dashed line is the standard deviation. Top is 151 mm amplitude (top) and 303 mm amplitude (bottom).

The ensemble average of these signals shown in Figure 4 indicates a predicted mean peak pressure of order

2 kPa for sensor #9 and 5.5 kPa for #10 both oscillation amplitudes. The standard deviation in the peak value is predicted to be 60-70% of the mean, indicating high variability. High deviation before the time of mean peak pressure is suggestive of variation in the timing of the fluid impact whereas high deviation with a narrow peak suggests high variation in peak magnitude. The maximum deviation occurs around the time of the mean peak pressure and drops rapidly after the mean peak (to approximately 30% of the mean pressure), suggesting that the pressure reduction after the peak follows a similar pattern after each impact. This is consistent with the shape of the pressure traces seen in Figure 3.

### 70% fill level

Results for the case of 70% fill in the transverse tank are presented in Figure 5 to Figure 7. Data was collected at all sensors #1-8. As with the 20% fill level, the results for the two different amplitudes are qualitatively quite similar (Figure 5). As the tank reaches maximum displacement to the left, the fluid has either just impacted the tank wall (151 mm amplitude), or has just formed a jet that moves along the upper filet (303 mm) (first row in Figure 5).

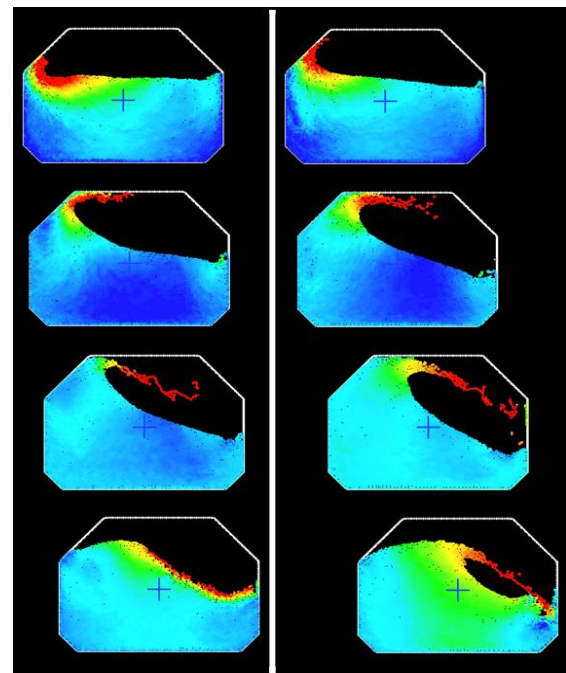


**Figure 5:** Fluid particle positions for the 70% fill level (with the 151 mm amplitude in the left column and the 303 mm amplitude in the right column). The first half of the oscillation period is shown as the tank moves from left to right. The maximum velocity (red) is associated with the jet and breaking wave tip and is  $4.0 \text{ ms}^{-1}$  for 151 mm and  $5.4 \text{ ms}^{-1}$  for 303 mm.

As the tank starts accelerating back to the right, the jet that has formed on the left-hand wall soon impacts the tank ceiling because of the high fill level. As the tank continues to move to the right, additional fluid builds up on the left-hand wall and the high pressure at the tank ceiling creates a jet that starts to move along the ceiling, however it soon falls under gravity. The general picture is similar to that of a breaking shore wave. For the 151 mm amplitude oscillation, the breaking wave impacts the surface of the fluid in the tank at about the  $\frac{3}{4}$  of maximum

amplitude to the right (last row in Figure 5) whereas for the 303 mm amplitude oscillation it impacts the opposite side wall of the tank at the location of the liquid surface.

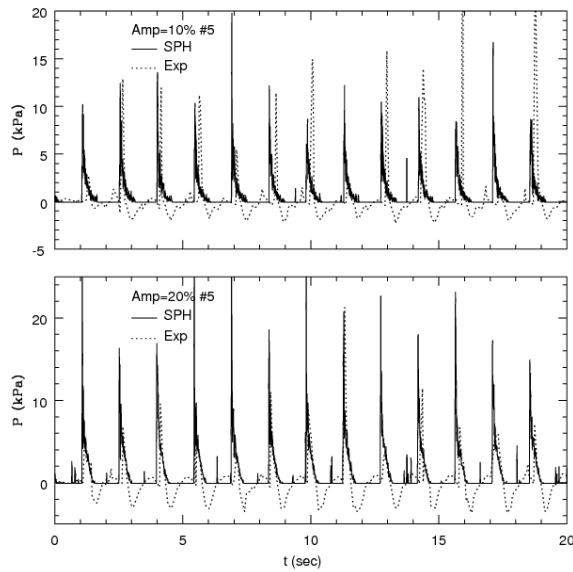


**Figure 6:** Pressure signal at start-up for at sensor locations #5 for 70% fill level in the transverse tank: 151 mm amplitude (top) and 303 mm amplitude (bottom). SPH results (solid line) are compared to experimental results (dashed line).

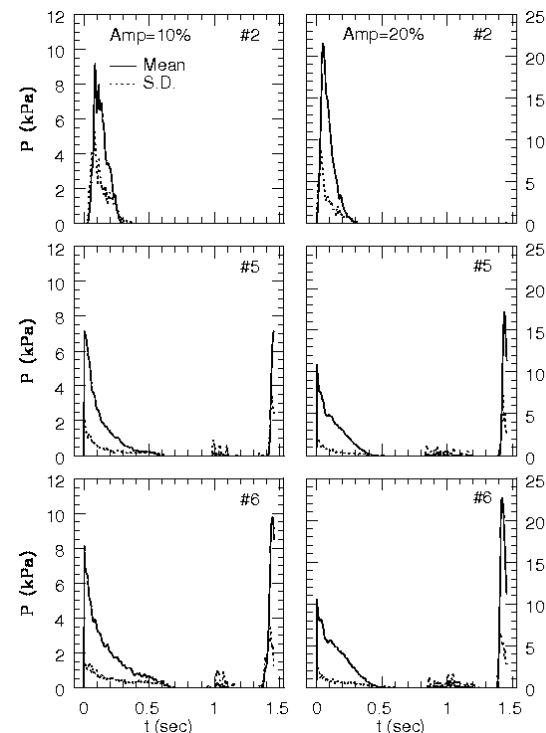


**Figure 7:** Ensemble averaged pressure trace and standard deviation for sensors #2, 5 and 6 for the transverse tank with 70% fill: Solid line is ensemble-averaged pressure trace and the dashed line is the standard deviation. Left is 151 mm amplitude and right is 303 mm amplitude.

The jet that forms on the left side of the tank as it comes to rest is associated with the high pressure seen in the ensemble-averaged pressure readings for sensor #5

(see Figure 7). The pressure peaks for sensor #5 (shown in Figure 6) appear to be generally under-predicted by about 25% for the 151 mm amplitude sloshing and over-predicted by about the same amount for the 303 mm amplitude.

The maximum predicted ensemble-averaged pressures occur at sensor #6 on the side wall with values of 10 kPa (23 kPa) for 151 mm (303 mm) amplitude. This peak is associated with the vertical wall jet being forced to change direction between sensors #7 and #6. The second highest mean reading is predicted to occur at sensor #2 at the ceiling just around from the upper fillet, with mean values of 9 kPa (21 kPa) for 151 mm (303 mm) amplitude. Again, this is associated with the angled wall jet being forced horizontal as it hits the tank ceiling.

The maximum standard deviation in pressure occurs at sensor #2 and is approximately 40% of the mean peak pressure and occurs just before the time of mean impact. At sensor #6 the standard deviation is about 30% of the mean peak pressure. At both these sensors, the standard deviation has dropped by one half by the time of the mean peak pressure, suggesting that a significant part of the signal variability is due to the timing of the impact.

#### Comparison between 20% and 70% fill levels

The two different fill levels have different oscillation frequencies and should therefore be compared with caution. Using the maximum observed simulation velocity,  $V$ , and the nominal height,  $H$ , from the free surface to the ceiling, for the 20% fill level the distance from the free surface to the ceiling is greater than  $V^2/2gH$  for both amplitude oscillations and thus we would not expect roof impacts as predicted in Figure 2. On the other hand, for the 70% fill level this distance is significantly smaller and we expect significant ceiling impact. Indeed this is the case as seen in Figure 5. The peak pressures should scale like the maximum velocity squared. Considering the time traces in Figure 3 and Figure 6, the peak values correspond approximately to this scaling ratio. However this is not apparent in the maximum ensemble averaged pressure values in which the peak pressures are averaged out due to variability in timing as well as magnitude. The variability in the pressure signal is predicted to be higher for the lower fill level, with the standard deviation in mean peak pressure being approximately 60-70% of the mean peak for low fill case compared to 40% in the higher fill case.

#### CONCLUSION

SPH is seen to capture the basics of liquid sloshing in two-dimensional water models of an LNG tank. The pressure signals are seen to be quasi-periodic, but the fluid surface changes with each cycle and results in pressure peaks that can vary substantially between impacts. Comparison of the pressure traces from SPH and some of those presented in Kim *et al.* (2009) show that the phase of the pressure signals is in quite good agreement with the experiments (which is to be expected), but that SPH generally under-predicts the peak pressure values by 20-30%, although in also over-predicts in some cases by similar amounts. The free-surface profiles were in reasonable qualitative agreement for many of the different sloshing cases (not shown), although entrainment of bubbles in the experiments (and their absence in the modelling) makes a good comparison difficult.

Suggested in this work is that the generation of high wall pressure is related to the impingement of liquid jets on the tank walls and most importantly by wall jets encountering a sudden change in geometry (e.g. a tank knuckle or corner). These high speed jets are caused by the general fluid impact arising from sloshing, although the primary sloshing impacts in themselves do not necessarily result in the highest pressures. This aspect of the modelling needs to be investigated further with a closer distribution of pressure sensors needed to better check the full distribution around the tank walls.

Despite the deterministic nature of the harmonic motion of the tank, the sloshing motion and consequent pressure traces contain a significant stochastic component. The origin of the stochastic behaviour is the high Reynolds number, free surface nature of the flow. It is unstable and hence highly irregular at small time and length scales. Hence, the suggestion that pressure traces resulting from impact could be numerically predicted with a 1:1 correspondence to experimental results is not realistic. However, what does seem feasible is that the stochastic nature of the sloshing impacts could be captured statistically, and the ensemble-averaged signals and associated standard deviations are one way in which a comparison could be made.

Ensemble-averaged pressure signals from the simulation results are presented here. They provide useful information about the pressure, although the peak information is lost in the process. There is seen to be higher variability in the peak pressure (i.e. higher standard deviation) for the 20% fill case as compared to the 70% fill. This higher variability can be caused both by higher variability in the peak pressures and in the exact timing of the maximum pressure. The predicted ensemble averaged pressure signals ideally need to be compared to similar experimental averages. This would then provide an indication of whether a computational technique is able to capture the important features of sloshing, especially relevant information on the maximum pressures and their statistical, spatial and temporal distribution.

The simulations here have only considered the presence of the liquid phase and the gas phase has been ignored. Including this in the computation is the main improvement to the model physics that is required. Its inclusion will modify both the fluid flow and predicted maximum pressures, and is currently under development in the SPH framework.

## REFERENCES

CLEARY, P. W., ‘Modelling confined multi-material heat and mass flows using SPH’, *Appl. Math. Modelling*, **22**, 981-993, (1998).

CLEARY, P.W., and PRAKASH, M., ‘Smooth Particle Hydrodynamics and Discrete Element Modelling: potential in the environmental sciences’, *Philosophical Transactions A*, **362**, 2003-2030, (2004).

CLEARY, P.W. and RUDMAN, M. ‘Extreme wave interaction with a floating oil rig’, *Progress in Comput. Fluid. Dyn.* **9** 332-334 (2009)

GERRITS, J, and VELDMAN, A.E.P., ‘Dynamics of liquid filled spacecraft’, *J. Eng. Mathematics* **45** 21-38 (2003).

GINGOLD, R.A. and MONAGHAN, J.J. *Mon. Not. Roy. Ast. Soc.* **181** 375 (1977).

GOMEZ-GESTEIRA, M., CERQUEIRO, D., CRESPO, C. and DALRYMPLE, R.A. ‘Green water overtopping analyzed with a SPH model’, *Ocean Eng.* **32** 223-238 (2005).

HIRT, C.W. and NICHOLS, B.D., ‘Volume of fluid (VOF) methods for the dynamics of free boundaries’, *J. Comput. Phys.* **39**, 201-225 (1981).

JUNG, J.-J., Lee, H.-H., PARK, T.-H. and LEE, Y.-W., ‘Experimental and numerical investigation into the effects of fluid-structure interaction on the sloshing impact loads in membrane LNG carrier’, *OMAE2008, 27<sup>th</sup> International Conference on Offshore Mechanics and Arctic Engineering* 15<sup>th</sup>-19<sup>th</sup> June 2008, Estoril Portugal.

KIM, H.I, KWON, S.H., PARK, J.S., LEE, K.H, JEON, S.S., JUNG, J.H., RYU, M.C. and HWANG, Y.S. ‘An Experimental Investigation of Hydrodynamic Impact on 2-D LNGC Models’, Paper YHK12, pp 30-37, *19<sup>th</sup> International Offshore and Polar Engineering Conference* June 21-26, 2009, Osaka, Japan.

MONAGHAN, J.J. ‘Simulating free surface flows with SPH’, *J. Comput. Phys.* **110L** 399-406 (1994).

RUDMAN, M, PRAKASH, M and CLEARY, P.W., ‘Simulation of Liquid Sloshing in a model LNG Tank using Smoothed Particle Hydrodynamics’ Paper YHK13, pp 213-220, *19<sup>th</sup> International Offshore and Polar Engineering Conference* June 21-26, 2009, Osaka, Japan.

SCHREIER, S. and PASCHEN, M., ‘Sloshing in LNG tanks – assessment of high and low pressures’, *OMAE2008, 27<sup>th</sup> International Conference on Offshore Mechanics and Arctic Engineering* 15<sup>th</sup>-19<sup>th</sup> June 2008, Estoril Portugal.

SHAO, S. ‘Incompressible SPH simulation of wave breaking and overtopping with turbulence modelling’, *Int. J. Numer. Meth. Fluids* **50** 597-621 (2006).

SINGH, S.P., LAL, A. and DHAVALIKAR, S.S. ‘Numerical prediction of sloshing loads in ship tanks’, *OMAE2008, 27<sup>th</sup> International Conference on Offshore Mechanics and Arctic Engineering* 15<sup>th</sup>-19<sup>th</sup> June 2008, Estoril Portugal.

M. SUSSMAN, P. SMEREKA and S. OSHER, ‘A level set approach for computing solutions to incompressible two-phase flow’, *J. Comput. Phys.*, **114**, 146-149 (1994)

VON BERGHEIM, P and THIAGARAJAN, K.P. ‘The air-water sloshing problem: parametric studies on excitation magnitude and frequency’, *OMAE2008, 27<sup>th</sup> International Conference on Offshore Mechanics and Arctic Engineering* 15<sup>th</sup>-19<sup>th</sup> June 2008, Estoril Portugal.

WEMMENHOVE, R., LUPPES, R., VELDMAN, A.E.P and BUNNIK, T., ‘Numerical simulation of sloshing in LNG tanks with a compressible two-phase model’, *OMAE2007, 26<sup>th</sup> International Conference on Offshore Mechanics and Arctic Engineering* 10<sup>th</sup>-15<sup>th</sup> June 2007, San Diego, California.